Geophysical Prospecting, 2006, **54**, 463–473

Theoretical development of the differential scattering decomposition for the 3D resistivity experiment

Greg A. Oldenborger[1]* and Partha S. Routh[2]

[1]*Department of Earth and Ocan Sciences, University of British Columbia, 6339 Stores Road, Vancouver, BC V6T 1Z4, Canada, and*
[2]*Department of Geosciences, Boise State University, 1910 University Drive, Boise ID 83725, USA*

Received May 2005, revision accepted January 2006

ABSTRACT

In any numerical solution of the DC resistivity experiment, care must be taken to deal with strong heterogeneity of electrical conductivity. In order to examine the importance of conductivity contrasts, we develop a scattering decomposition of the DC resistivity equation in the sparse differential domain as opposed to the traditional dense integral formulation of scattering-type equations. We remove the singularity in the differential scattered series via separation of primary and secondary conductivity, thereby avoiding the need to address the singularity in a Green's function. The differential scattering series is observed to diverge for large conductivity contrasts and to converge for small contrasts. We derive a convergence criterion, in terms of matrix norms for the weak-form finite-volume equations, that accounts for both the magnitude and distribution of heterogeneity of electrical conductivity. We demonstrate the relationship between the differential scattering series and the Fréchet derivative of the electrical potential with respect to electrical conductivity, and we show how the development may be applied to the inverse problem. For linearization associated with the Fréchet derivative to be valid, the perturbation in electrical conductivity must be small as defined by the convergence of the scattered series. The differential scattering formulation also provides an efficient tool for gaining insight into charge accumulation across contrasts in electrical conductivity, and we present a derivation that equates accumulated surface charge density to the source of scattered potential.

INTRODUCTION

The solution of the low-frequency (DC) resistivity equation for the electrical potential distribution, given a general electrical conductivity field, can be approached from a variety of directions. To allow for the discretization of arbitrary three-dimensional (3D) earth models, a finite-difference or finite-element approximation of the governing differential equation is usually used (Li and Spitzer 2002). Whichever numerical method is chosen for solving the differential equation, care must be taken to deal with strong heterogeneity of electrical conductivity. For example, Spitzer and Wurmstich (1999) provided a review of 3D finite-difference techniques in the context of the DC resistivity problem and they demonstrated that the main discrepancies in numerical results stem from the different approaches used to handle discontinuities in electrical conductivity.

We investigate the role of contrasts in electrical conductivity by describing the behaviour of the potential solution using a scattering decomposition. The development is unique in that we formulate the scattered series in the differential domain as opposed to the traditional integral formulation of scattering-type equations. This is significant in that large 3D problems with general electrical conductivity distributions are almost invariably solved using a numerical approximation of the differential equation, not the integral equation.

*E-mail: goldenborger@eos.ubc.ca

Finite-difference matrices are sparse, easily generated, and efficiently stored. Conversely, integral techniques involve costly calculation, storage, and integration of a dense Green's function. Furthermore, the singularity of the Green's function must be addressed in integral techniques (Snyder 1976), whereas we use the elegant separation of primary and secondary potential of Lowry, Allen and Shive (1989) to address the singularity in the differential domain. Once formulated, the differential scattering series provides useful insight into the DC resistivity experiment with regard to the validity of the Born approximation, the applicability of the Fréchet derivative, and the charge accumulation at conductivity contrasts.

We begin with a brief discussion of the forward problem using a weak formulation and we show how the differential scattering series results from a separation of primary and secondary conductivity. Following this, we implement the scattering decomposition for a synthetic 3D example and develop a convergence criterion for the scattered series. We then discuss ways in which the scattering decomposition and the associated convergence behaviour may be applied to the non-linear DC resistivity inverse problem and we present a field example for a 3D electrical resistivity tomography experiment. Finally, we illustrate the relationship between the secondary potential and surface charge accumulation.

FORWARD MODEL

The differential equation and boundary condition describing the DC resistivity experiment are given by

$$-\nabla \cdot [\sigma(\mathbf{r})\nabla\phi(\mathbf{r})] = I\delta(\mathbf{r}-\mathbf{r}_s) \qquad \text{within } V, \tag{1a}$$

$$\alpha(\mathbf{r})\phi + \beta(\mathbf{r})\partial\phi/\partial n = 0 \qquad \text{on } S, \tag{1b}$$

where ϕ is the electrical potential, σ is the electrical conductivity, $I\delta(\mathbf{r}-\mathbf{r}_s)$ is the pole-source function with current strength I, $\mathbf{r} = x\hat{\mathbf{i}} + y\hat{\mathbf{j}} + z\hat{\mathbf{k}}$ is the receiver position vector, $\mathbf{r}_s = x_s\hat{\mathbf{i}} + y_s\hat{\mathbf{j}} + z_s\hat{\mathbf{k}}$ is the source position vector, $\mathbf{n}$ is the outward normal vector to the surface boundary S of domain V, and α and β are factors dictated by the specific boundary conditions. Since the differential operator is linear in ϕ, the response to any source array can be built from a summation of solutions for a series of pole sources (i.e. the principle of superposition). In this case, we consider the conductivity to be purely real and independent of frequency. However, our methods and results are easily generalized to complex conductivity.

The forward problem for the DC resistivity experiment is very often solved using finite-elements (Li and Spitzer 2002), Taylor series expansion with finite-difference approximation (Spitzer 1995), or a weak-form finite-volume approximation (Dey and Morrison 1979). The weak-form expression of the DC resistivity equation is developed by integrating the differential equation (1a) over some small elemental volume and applying the divergence theorem, such that

$$-\int_S \sigma\nabla\phi \cdot \hat{\mathbf{n}}\,\mathrm{d}S = I(x_s, y_s, z_s). \tag{2}$$

The weak-form equation (2) demands only first-order differentiability of the potential and can thus be solved for any medium with a piecewise continuous potential, a discontinuous source function, and discontinuous conductivity, which allows for strongly heterogeneous earth models.

We discretize (2) using a finite-volume technique whereby the surface integral is evaluated in a piecewise fashion over the entire computational domain. The potential gradient within the surface integral is evaluated using a centred, second-order finite-difference approximation, which casts the surface integral in terms of neighbouring node potentials. The result is a system of linear algebraic equations expressed as $\mathbf{Cv} = \mathbf{b}$, where $\mathbf{v}$ is the vector of node potentials, $\mathbf{b}$ is the source vector and $\mathbf{C}$ is the coupling matrix, which is sparse, 7-banded, positive definite, and symmetric. The zero-flux (Neumann-type) boundary condition for the potential is easily incorporated into $\mathbf{C}$ for model elements at the earth's surface. At other domain boundaries, we use a source-dependent, mixed (Robin-type) boundary condition (Zhou and Greenhalgh 2001). We solve for the node potentials as $\mathbf{v} = \mathbf{C}^{-1}\mathbf{b}$, where the coupling matrix is inverted using a stabilized biconjugate gradient solver (Press *et al.* 1992), preconditioned using symmetric successive overrelaxation (Golub and Van Loan 1996).

SECONDARY FORMULATION

Much of the error in modelling the DC resistivity experiment arises from the singularity associated with the point source of current. Lowry *et al.* (1989) presented a method of analytically removing this singularity by invoking a separation of the primary (ϕ^P) and secondary (ϕ^S) potentials in response to perturbation of the primary conductivity (σ^P) by the secondary conductivity (σ^S). We consider the primary conductivity to be homogeneous and equal to the conductivity at the source location (Zhao and Yedlin 1996). Substitution into the DC resistivity equation yields

$$-\nabla \cdot [(\sigma^P + \sigma^S)\nabla(\phi^P + \phi^S)] = I\delta(\mathbf{r}-\mathbf{r}_s), \tag{3}$$

which, after subtraction of the primary solution and grouping of the secondary potential terms, leads to the equation for secondary potential,

$$-\nabla \cdot [\sigma \nabla \phi^{\mathrm{S}}] = \nabla \cdot [\sigma^{\mathrm{S}} \nabla \phi^{\mathrm{P}}]. \tag{4}$$

Again, we solve the differential system via weak-form integration of both the forward and source operators as

$$-\int_S \sigma \nabla \phi^{\mathrm{S}} \cdot \hat{\mathbf{n}}\, \mathrm{d}S = \int_S \sigma^{\mathrm{S}} \nabla \phi^{\mathrm{P}} \cdot \hat{\mathbf{n}}\, \mathrm{d}S, \tag{5}$$

for which the primary potential is solved analytically, thereby accounting for the singularity associated with the point source.

In terms of the discrete weak-form equations, (5) is expressed as $\mathbf{C}\mathbf{v}^{\mathrm{S}} = -\mathbf{C}^{\mathrm{S}}\mathbf{v}^{\mathrm{P}}$, where $\mathbf{C}^{\mathrm{S}}$ is the secondary coupling matrix, built using the secondary conductivity (Spitzer, Chouteau and Boulanger 1999; Wu *et al.* 2003), and the primary potential is evaluated analytically using the conductivity at a given source location. We solve the linear algebraic system for the secondary potential in the same manner as the full potential equation but with a new source term.

Figure 1 shows estimated apparent conductivities compared with the analytical solution for a vertical dike model (e.g. Telford, Geldart and Sheriff 1990). The secondary solution demonstrates a marked increase in accuracy over the full potential solution. There are some fluctuations of the secondary solution at conductivity boundaries, but these fluctuations are much lower in magnitude than the error associated with the full potential solution. If the resistivity of the dike is increased by an order of magnitude, the secondary errors approach 2% over the dike (not shown). That is, when the source is located in the conductor, errors associated with the secondary formulation increase, as shown by McGillivray (1992). However, the accuracy is still significantly greater than that for the full potential solution. In the following section, we use the secondary potential for an initial examination of the scattering nature of compact heterogeneities. Following that, we extend the results to general conductivity distributions in the context of the inverse problem.

SCATTERING DECOMPOSITION

The secondary potential equation (4) shows, in effect, that the source of the secondary potential is a current density resulting from charge accumulation at conductivity contrasts; this is a scattering-type equation in the differential domain and we can use it to construct a scattering series solution for the potential field.

As a first attempt, we separate all terms in (4) and rearrange them to yield

$$-\nabla \cdot [\sigma^{\mathrm{S}} \nabla \phi^{\mathrm{S}}] = \nabla \cdot [\sigma^{\mathrm{S}} \nabla \phi^{\mathrm{P}}] + \nabla \cdot [\sigma^{\mathrm{P}} \nabla \phi^{\mathrm{S}}]. \tag{6}$$

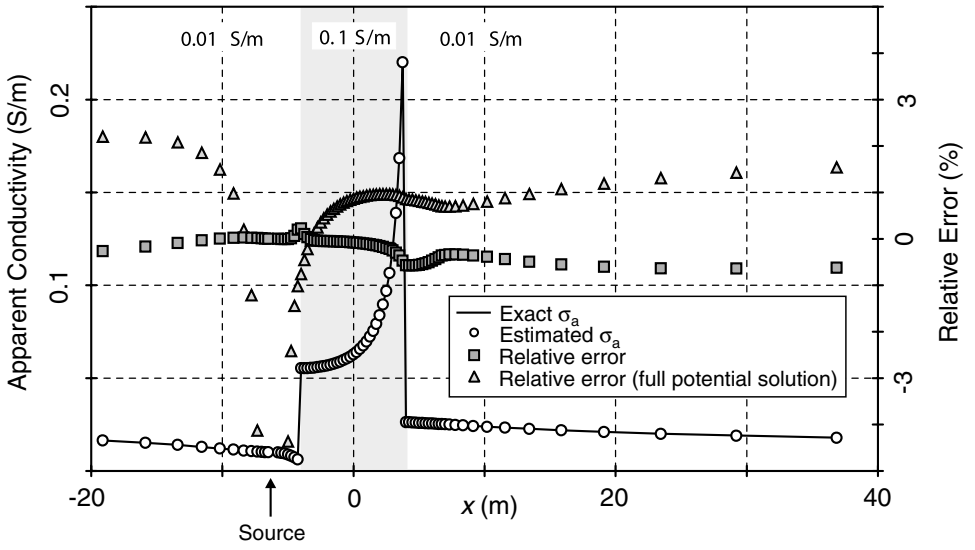

Figure 1 Pole-dipole apparent conductivities estimated using a secondary potential formulation for a conductive dike model. The background conductivity is 0.01 S/m and the dike conductivity is 0.1 S/m from $x = -4$ to 4 m. The current source is of unit strength at $x = -6$ m, $y = 0$ m, $z = 0$ m and the illustrated profile is at $y = 0$ m, $z = 0$ m. The numerical grid has a regular 0.25 m spacing that changes to a variable outward-increasing spacing from 7 to ~200 m in the x-direction and from 2 to ~200 m in the y- and z-directions. The positive error indicates overestimation of the true apparent conductivity.

We let $\phi_0 = \phi^{\mathrm{P}}$ and $\phi_0^{\mathrm{S}} = 0$, and we construct the scattering series as

$$\begin{aligned}
&-\nabla \cdot \left[\sigma^{\mathrm{S}} \nabla \phi_1^{\mathrm{S}}\right] = \nabla \cdot [\sigma^{\mathrm{S}} \nabla \phi^{\mathrm{P}}], \quad \phi_1 = \phi^{\mathrm{P}} + \phi_1^{\mathrm{S}}, \\
&-\nabla \cdot \left[\sigma^{\mathrm{S}} \nabla \phi_2^{\mathrm{S}}\right] \\
&\quad = \nabla \cdot [\sigma^{\mathrm{S}} \nabla \phi^{\mathrm{P}}] + \nabla \cdot [\sigma^{\mathrm{P}} \nabla \phi_1^{\mathrm{S}}], \quad \phi_2 = \phi^{\mathrm{P}} + \phi_2^{\mathrm{S}} \quad , \ldots, \\
&-\nabla \cdot [\sigma^{\mathrm{S}} \nabla \phi_j^{\mathrm{S}}] \\
&\quad = \nabla \cdot [\sigma^{\mathrm{S}} \nabla \phi^{\mathrm{P}}] + \nabla \cdot \left[\sigma^{\mathrm{P}} \nabla \phi_{j-1}^{\mathrm{S}}\right], \quad \phi_j = \phi^{\mathrm{P}} + \phi_j^{\mathrm{S}},
\end{aligned} \tag{7}$$

where ϕ_j^{S} is the jth-order scattered potential and ϕ_j is the jth-order approximation to the full potential. However, this series suffers from the fact that, in the formation of the system,

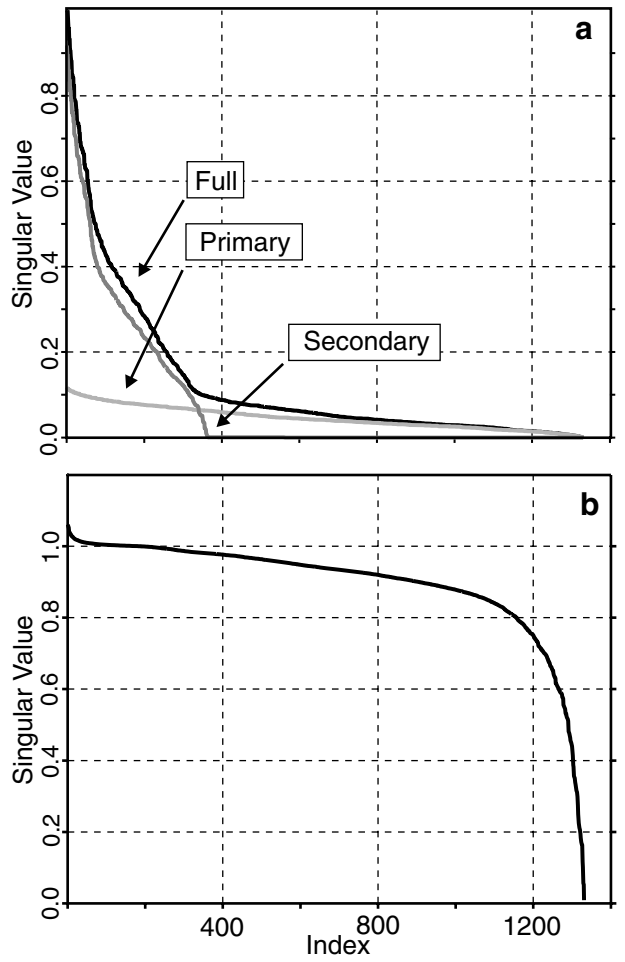

Figure 2 Singular value spectra for (a) the full, primary and secondary weak- form differential operators $\mathbf{C}$, $\mathbf{C}^{\mathrm{P}}$ and $\mathbf{C}^{\mathrm{S}}$, and (b) the preconditioned form of $\mathbf{C}$ for a small earth model of 1331 nodes and 1000 cells, 200 of which represent a conductive dike (secondary conductivity) with a conductivity contrast of a factor of ten. The preconditioned form of $\mathbf{C}^{\mathrm{P}}$ is indistinguishable from that of $\mathbf{C}$ at the scale shown.

$\mathbf{C}^{\mathrm{S}}\mathbf{v}_j^{\mathrm{S}} = -\mathbf{C}^{\mathrm{S}}\mathbf{v}^{\mathrm{P}} - \mathbf{C}^{\mathrm{P}}\mathbf{v}_{j-1}^{\mathrm{S}}$, the secondary operator $\mathbf{C}^{\mathrm{S}}$ is considerably more sparse than either the full operator $\mathbf{C}$ or the primary operator $\mathbf{C}^{\mathrm{P}}$. In fact, $\mathbf{C}^{\mathrm{S}}$ is only semi-positive definite and cannot be inverted, as illustrated in Fig. 2 by the singular-value spectra for a small problem.

Alternatively, we can separate the terms of (4) and group the secondary conductivity terms to yield

$$-\nabla \cdot [\sigma^{\mathrm{P}} \nabla \phi^{\mathrm{S}}] = \nabla \cdot [\sigma^{\mathrm{S}} \nabla \phi]. \tag{8}$$

Again, we let $\phi_0 = \phi^{\mathrm{P}}$ and $\phi_0^{\mathrm{S}} = 0$, and we construct the scattered series as

$$\begin{aligned}
&-\nabla \cdot \left[\sigma^{\mathrm{P}} \nabla \phi_1^{\mathrm{S}}\right] = \nabla \cdot \left[\sigma^{\mathrm{S}} \nabla \phi_0\right], \quad \phi_1 = \phi_0 + \phi_1^{\mathrm{S}}, \\
&-\nabla \cdot \left[\sigma^{\mathrm{P}} \nabla \phi_2^{\mathrm{S}}\right] = \nabla \cdot \left[\sigma^{\mathrm{S}} \nabla \phi_1\right], \quad \phi_2 = \phi_0 + \phi_2^{\mathrm{S}}, \quad \ldots, \\
&-\nabla \cdot \left[\sigma^{\mathrm{P}} \nabla \phi_k^{\mathrm{S}}\right] = \nabla \cdot \left[\sigma^{\mathrm{S}} \nabla \phi_{k-1}\right], \quad \phi_k = \phi_0 + \phi_k^{\mathrm{S}},
\end{aligned} \tag{9}$$

where ϕ_k^{S} is the kth-order scattered potential and ϕ_k is the kth-order approximation to the full potential. In the event that the series converges, the scattered potential approaches the total secondary potential as $k \to \infty$. Conversely, the first term of the scattering series ($k = 1$) represents the familiar Born approximation, whereby a change in the potential is expressed as a first-order linear mapping with a conductivity perturbation. The approximate first-order scattering solution will be meaningful when electrical conductivity variations are weak compared to the background; we expect this approximation to be inadequate for realistic conductivity contrasts (Hohmann and Raiche 1988).

We implement the scattering series (9) in the 3D discrete weak form as $\mathbf{C}^{\mathrm{P}}\mathbf{v}_k^{\mathrm{S}} = -\mathbf{C}^{\mathrm{S}}\mathbf{v}_{k-1}$. Figure 3 illustrates the first- and second-order scattering terms for the conductive dike model of Fig. 1 with an order of magnitude conductivity contrast. Clearly, the differential series diverges quite strongly in this case. Conversely, Fig. 4 illustrates the first- and second-order scattering terms for the conductive dike model of Fig. 1 with a conductivity contrast of a factor of only two. In this low-contrast case, the differential series is observed to converge with good agreement of the total estimated potential for $k \gtrsim 4$. For this particular dike model, convergence is limited by a conductivity contrast of less than a factor of approximately two; for greater contrasts, the series diverges. As expected, convergence of the scattering series is strongly model-dependent, both in terms of the magnitude of the secondary conductivity and the distribution of secondary conductivity over space.

For a better understanding of the convergence behaviour, we note that convergence or divergence of the differential scattering series is due, in large part, to the first-order scattered term.

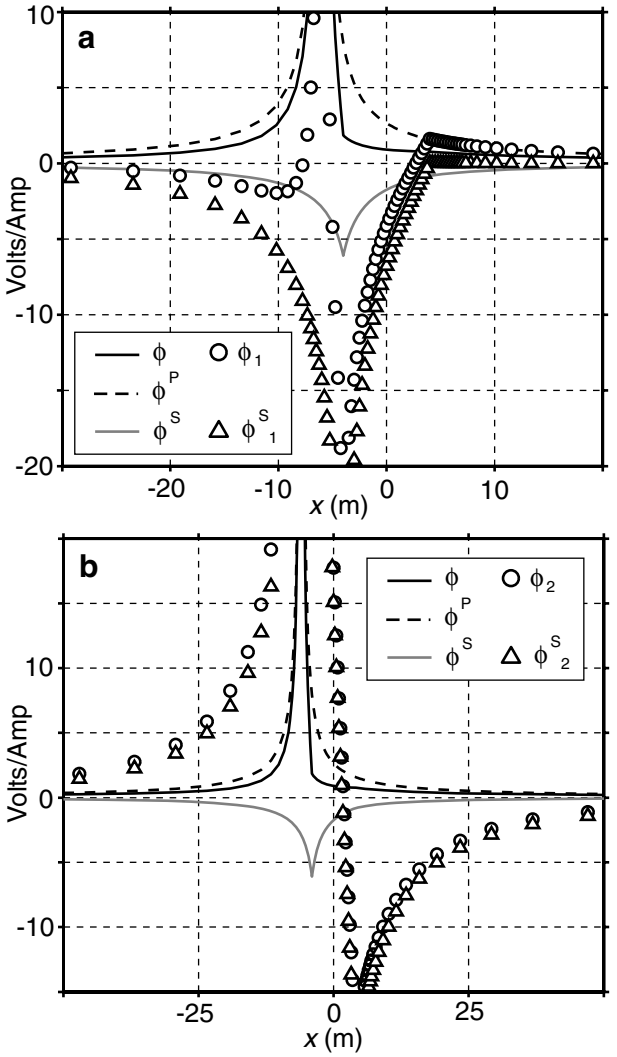

Figure 3 (a) First- and (b) second-order scattered potential terms for the dike model of Fig. 1. The illustrated profile is at $y = 0$ m, $z = 0$ m.

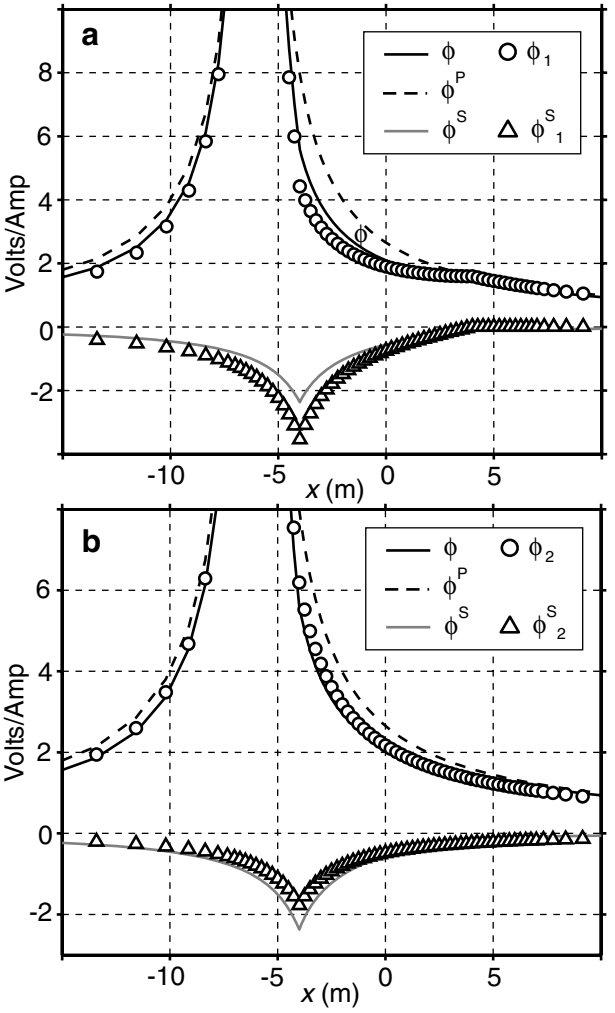

Figure 4 (a) First- and (b) second-order scattered potential terms for the dike model of Fig. 1 with a conductivity contrast of a factor of two. The illustrated profile is at $y = 0$ m, $z = 0$ m.

Comparing the first term of the series (9) with the secondary equation (4), we see that the source functions are identical. Thus, the error associated with the first-order scattered potential (an approximation to the total secondary potential) stems from the primary forward operator of (9), which is a smooth Laplacian operator since σ^{P} is homogeneous. By expanding the source function, we see $\nabla \cdot [\sigma^{\mathrm{S}} \nabla \phi^{\mathrm{P}}] = \sigma^{\mathrm{S}} \nabla^2 \phi^{\mathrm{P}} + \nabla \sigma^{\mathrm{S}} \cdot \nabla \phi^{\mathrm{P}}$, which is only non-zero for non-zero secondary conductivity and conductivity gradient. Although not generally true, the product of the secondary conductivity and the Laplacian of the primary potential ($\sigma^{\mathrm{S}} \nabla^2 \phi^{\mathrm{P}}$) tends to be small in comparison with the scalar product of the secondary conductivity gradient and the primary potential gradient ($\nabla \sigma^{\mathrm{S}} \cdot \nabla \phi^{\mathrm{P}}$), so that the source function tends to be large at conductivity contrasts, as illustrated in Fig. 5 for the dike model. However, for convergence, the scattering series requires that the source term diminishes in strength with each order. Since σ^{S} is constant over the series, the requirement for convergence is that ϕ_1 be smoother than ϕ_0 over the regions of non-zero σ^{S}.

Theoretically, the tendency to converge or diverge is captured entirely by the coupling matrices, and we show that the differential series converges in the event that $||(\mathbf{C}^{\mathrm{P}})^{-1}\mathbf{C}^{\mathrm{S}}|| \lesssim 1$ or the spectral radius of $(\mathbf{C}^{\mathrm{P}})^{-1}\mathbf{C}^{\mathrm{S}}$ is less than unity (see Appendix); this is a convergence criterion for the differential scattering series and is, in effect, a validity criterion for the Born approximation. As the conductivity contrast decreases (in magnitude and distribution), the singular value spectra of the secondary and full operators diverge while the spectra

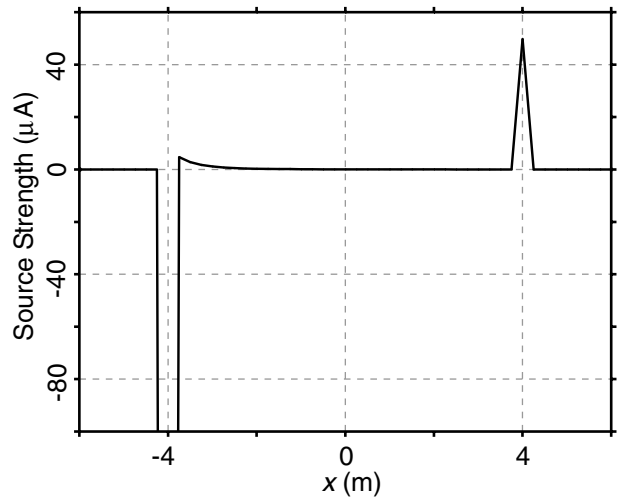

Figure 5 First-order weak-form source term at $y = 0$ m, $z = 0$ m for the scattering series associated with the dike model of Fig. 1 with a contrast conductivity of a factor of two. The maximum source magnitude is -1.3 mA (not shown); the large source magnitude indicates high surface charge density. The source magnitude increases with increased contrast conductivity but the shape of the source term remains constant.

of the primary and full operators converge. The secondary matrix becomes weaker and increasingly sparse (along the diagonal), thereby significantly lowering the combined matrix norm. This formulation of the convergence criterion in terms of the coupling matrices accounts for variability in both the magnitude and distribution of conductivity contrasts, the source location (via the choice of primary conductivity), and even the properties of the numerical mesh, but it may be less intuitive than the previous arguments of smoothness.

Implications for the Fréchet derivative

The inverse problem for the DC resistivity experiment is nonlinear due to the dependence of the forward operator on the model parameter of interest, i.e. the electrical conductivity. Therefore, the inverse problem is usually linearized and solved in an iterative fashion (Spitzer 1995; Li and Oldenburg 2000). In calculating the Fréchet derivative (sensitivity) for linearized inversion of DC resistivity data, the procedure is very similar to that of secondary potential separation, but with the important distinction that the effect of the perturbation is linearized. In fact, for small perturbations, the Born approximation is equivalent to the Fréchet derivative as shown below.

We define the continuous differential operator $\mathcal{L}\{\,\} \equiv -\nabla \cdot [\sigma(\mathbf{r})\nabla\{\,\}]$ and proceed by perturbing the operator to obtain an equation that satisfies $\mathcal{L}\{\delta\phi\} + \delta\mathcal{L}\{\phi\} = 0$. Implicit in this perturbation technique is the goal of isolating a parameter perturbation from $\delta\mathcal{L}$ in order to construct a Fréchet kernel of the form, $\delta\phi(\mathbf{r}) = \int_{V'} F(\mathbf{r}, \mathbf{r}', m)\delta\sigma(\mathbf{r}')\,\mathrm{d}V'$.

For the resistivity equation (1), the perturbed (or variational) form is given by

$$-\nabla \cdot [(\sigma + \delta\sigma)\nabla(\phi + \delta\phi)] = I\delta(\mathbf{r} - \mathbf{r}_s), \tag{10}$$

which is equivalent to (3). If we expand the perturbation equation and subtract the unperturbed solution, we are left with

$$-\nabla \cdot [\sigma\nabla\delta\phi] = \nabla \cdot [\delta\sigma\nabla(\phi + \delta\phi)], \tag{11}$$

which is equivalent to the scattering equation (8). However, in order to obtain the form, $\mathcal{L}\{\delta\phi\} = -\delta\mathcal{L}\{\phi\}$, we must neglect the product of perturbed quantities ($\delta\sigma\nabla\delta\phi$) to yield the linearized (first-order) approximation,

$$-\nabla \cdot [\sigma\nabla\delta\phi] \approx \nabla \cdot [\delta\sigma\nabla\phi], \tag{12}$$

from which the Fréchet kernel is constructed (McGillivray and Oldenburg 1990). We note that (12) is equivalent to the first term of the scattered series (9) since, in the perturbation notation, ϕ and σ are the unperturbed or primary quantities. Because we have demonstrated that the first term of the series (9) is a valid representation of the scattered potential only under certain convergence conditions involving the magnitude and distribution of perturbed conductivity, we can expect the same for (12) and, by extension, any Fréchet derivative obtained from it.

However, many practical sensitivity calculations avoid the use of an explicit conductivity perturbation and instead they are implemented for infinitesimal perturbations using an adjoint Green's function solution or a sensitivity equation technique (e.g. McGillivray and Oldenburg 1990; Spitzer 1998). Nevertheless, perturbation size is important during the model update stage of the iterative inversion process. Any linearized model update will only be valid for perturbations that are sufficiently small for the first-order scattered term to be a reasonable approximation to the true scattered potential.

Application to an electrical resistivity tomography experiment

For an iterative inversion scheme, at any iteration i we have the potential distribution ϕ^i (primary potential), the conductivity model σ^i (primary conductivity), the model update $\Delta\sigma^i$ (secondary conductivity), the updated model σ^{i+1}, and the resulting potential distribution ϕ^{i+1}. The scattering series (9) can

then be recast as

$$
\begin{aligned}
&-\nabla\cdot\left[\sigma^i\nabla\phi_1^{\mathrm{S}}\right]=\nabla\cdot[\Delta\sigma^i\nabla\phi^i],\quad \tilde{\phi}_1^{i+1}=\phi^i+\phi_1^{\mathrm{S}},\\
&-\nabla\cdot\left[\sigma^i\nabla\phi_2^{\mathrm{S}}\right]=\nabla\cdot\left[\Delta\sigma^i\nabla\tilde{\phi}_1^{i+1}\right],\quad \tilde{\phi}_2^{i+1}=\phi^i+\phi_2^{\mathrm{S}},\ \ldots,\ (13)\\
&-\nabla\cdot\left[\sigma^i\nabla\phi_k^{\mathrm{S}}\right]=\nabla\cdot\left[\Delta\sigma^i\nabla\tilde{\phi}_{k-1}^{i+1}\right],\quad \tilde{\phi}_k^{i+1}=\phi^i+\phi_k^{\mathrm{S}},)
\end{aligned}
$$

where the model update $\Delta\sigma^i$ represents the scatterer strength, ϕ_k^{S} is the kth-order scattered potential (secondary potential), $\tilde{\phi}_k^{i+1}$ is the kth-order estimate of the updated potential and we have used the initial conditions $\tilde{\phi}_0^{i+1}=\phi^i$ and $\phi_0^{\mathrm{S}}=0$. Given convergence of the scattering series, $\tilde{\phi}_k^{i+1}$ approaches ϕ^{i+1} as $k\to\infty$. We note that an alternative formulation of the scattered series involves embedding the model update in a homogeneous background. However, this homogeneous approach assumes implicitly that the non-linearity of the problem is entirely the result of the model update or the scatterer distribution. In the approach presented here, the primary model σ^i is not necessarily homogeneous and, thus, non-linearity associated with the primary model is inherent.

In order to examine the applicability of the differential scattered series (13), we consider the results of a 3D electrical resistivity tomography (ERT) experiment carried out to simulate the detection and monitoring of the pump-and-treat remediation of a conductive contaminant in a near-surface alluvial aquifer. Figure 6 illustrates the estimated conductivity model realized after ten iterations of a Gauss–Newton inversion (Li and Oldenburg 2000) using the DCIP3D software (DCIP3D 2004). The starting (reference) model is a two-layer water-table model with the water table at a depth of 1.9 m, a vadose zone conductivity of 0.20 mS/m and a saturated conductivity of 1.5 mS/m.

This large 3D ERT problem consists of over 250 000 elements, thus formation of the coupling matrix convergence criterion is computationally impractical. Alternatively, we can test for convergence of the scattering decomposition (13) at any given iteration. We consider the first iteration, for which the model update (from the reference model) is illustrated in Fig. 7. The associated first- and third-order scattered

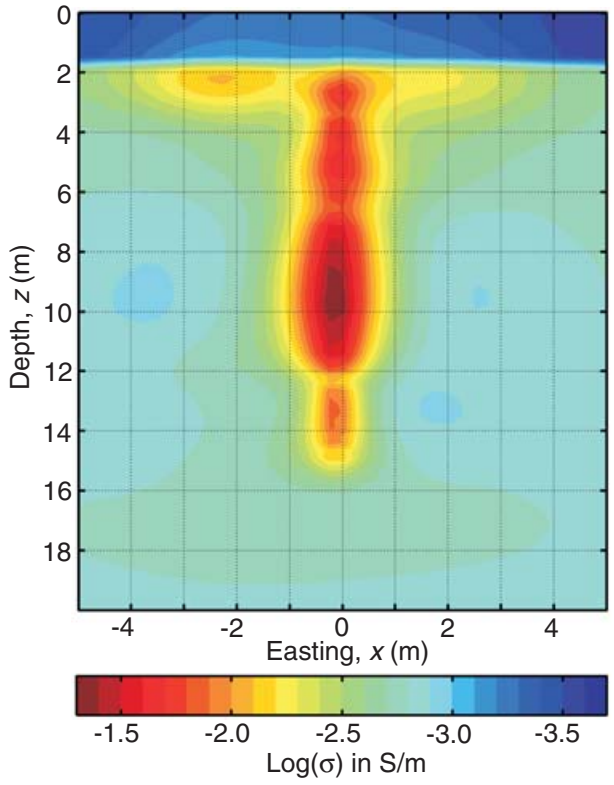

Figure 6 Final 3D conductivity model realized after ten iterations of a linearized Gauss–Newton inversion of ERT data. The conductivity model is relatively symmetrical in the horizontal plane and is shown sliced at $y=0$ m.

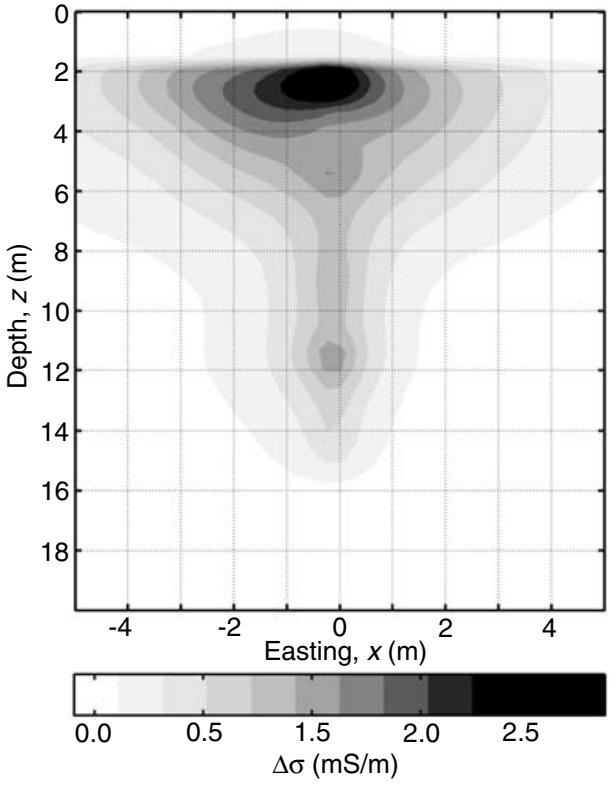

Figure 7 Magnitude of the first model update in the iterative inversion scheme. The model update is relatively symmetrical in the horizontal plane and is shown sliced at $y=0$ m. The first model update is applied to the two-layer initial (reference) model.

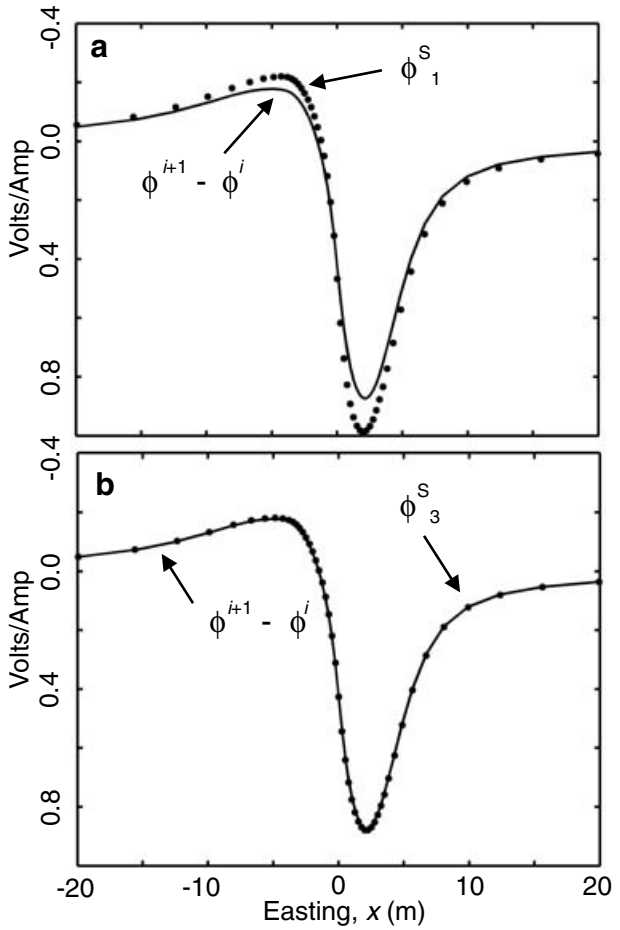

Figure 8 Dots indicate the (a) first- and (b) third-order scattered (secondary) potentials at $y = 0$ m, $z = 8$ m for the first model update illustrated in Fig. 7. Solid lines represent the exact scattered potential given by the difference between the primary and updated potentials.

potentials are extracted along the x-direction in Fig. 8 for a single pole source at the location, $x = 3$ m, $y = 3$ m, $z = 8$ m. For this example, the first-order scattered potential is a reasonable approximation to the exact scattered potential, computed as the difference between the updated and primary potentials; full convergence is achieved for $k \approx 3$. Given the good first-order agreement and rapid convergence of the scattered potential, and realizing that the initial steps in an iterative inversion scheme are often large and approximate, we can be reasonably certain that this particular model update is valid within the linearized inversion. A full assessment of the validity of the model update would require a similar analysis over all space for all sources in the ERT experiment.

A 2D slice of the first-order scattering source function is illustrated in Fig. 9 at a depth of 2 m above the source depth. In this case, the secondary conductivity $\Delta\sigma^i$ is not compact and is

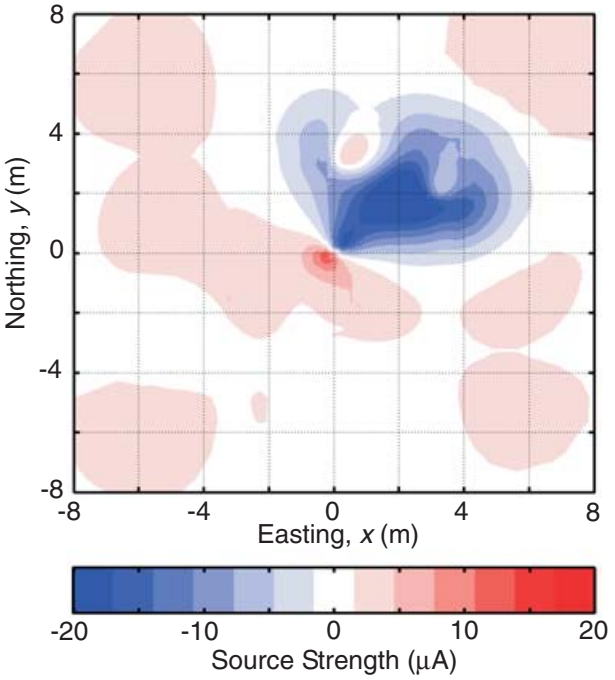

Figure 9 First-order scattering source strength at $z = 6$ m for the first model update illustrated in Fig. 7.

non-zero at the source location, so that the primary potential gradient $\nabla\phi^i$ is not nullified at the source point. In turn, the scattering source function is strongly influenced by the source location. Furthermore, contrary to the dike example, there is no sharp demarcation of the scattering (secondary) conductivity; it is distributed and diffuse (Fig. 7) due largely to the regularization inherent in the inversion procedure. Therefore, the scattering source function cannot easily be interpreted in terms of the spatial distribution of conductivity changes.

Charge accumulation

The implementation of the scattering equations (9) are discrete representations of the weak-form expression,

$$-\int_S \sigma^{\mathrm{P}} \nabla\phi_k^{\mathrm{S}} \cdot \hat{\mathbf{n}}\, \mathrm{d}S = \int_S \sigma^{\mathrm{S}} \nabla\phi_{k-1} \cdot \hat{\mathbf{n}}\, \mathrm{d}S. \tag{14}$$

As illustrated by the scattering series for the dike model (Fig. 5), the source function on the right-hand side of (14) is typically largest at conductivity contrasts for compact models. For distributed models, such as in the inversion example above, the scattering source function is not so easily interpreted (Fig. 9). The physical implication of (14) is that surface charges can accumulate when the electric field is perpendicular parallel to a conductivity contrast (Li and Oldenburg 1991).

The phenomenon of charge accumulation across contrasts in electrical conductivity (essentially a scattering problem) is commonly formulated as a Fredholm integral equation of the second kind (Snyder 1976). Alternatively, we can utilize the differential operators to calculate the accumulated charge density and the associated source function for the anomalous potential. To show that the source terms of the scattered series are indeed charge accumulations, we consider the expression for surface charge density τ of Li and Oldenburg (1991), cast in our notation:

$$\tau = -\epsilon_0 \frac{\sigma^{\mathrm{S}}}{\sigma} \nabla\phi \cdot \hat{\mathbf{n}}. \tag{15}$$

We can use the expression for surface charge density to rewrite (14) as

$$-\int_S \sigma^{\mathrm{P}} \nabla\phi_k^{\mathrm{S}} \cdot \hat{\mathbf{n}}\, \mathrm{d}S = -\int_S \frac{\sigma}{\epsilon_0} \tau_{k-1}\, \mathrm{d}S. \tag{16}$$

Considering the source function of (16), we see that the scattering series (9) can be related to the constructive and destructive superposition of potentials generated from the accumulated charge at the surface of a conductivity contrast. In practice, we measure the total potential, which has contributions from the primary potential and the infinite-order scattered potential (the secondary potential).

It is also possible to generate a discrete-form coupling matrix to relate the surface charge density across an interface to the secondary potential as $\mathbf{Bt} = \mathbf{C}^{\mathrm{P}}\mathbf{v}^{\mathrm{S}}$, where $\mathbf{B}$ is the discrete form of the right-hand surface integral of (16), $\mathbf{t}$ is the vector of surface charge densities, and the secondary potential $\mathbf{v}^{\mathrm{S}}$ is found via the solution of the discrete form of (5). However, in numerical implementations, care must be taken to honour the implicit dimensionality of the surface charge density, which resides at computational surfaces. It cannot be treated identically to ϕ, which resides at computational nodes, unless only an average surface charge density is required. Thus, in the numerical differential domain, the disparity in dimensionality between surface charge density and potential must be accounted for, possibly via averaging.

CONCLUDING DISCUSSION

Scattering formulations for electrical and electromagnetic experiments are typically implemented in an integral form. It is well known that such integrals can be very expensive to compute for large problems and they require detailed treatment of the singularity of the Green's function. The differential operators for the DC resistivity experiment, however, are sparse, easy to compute and efficient to store, and thereby provide an alternate method of examining the scattered potential.

As expected, the weak-form differential scattered series for electrical potential is observed to diverge for realistic contrasts in electrical conductivity. However, for small conductivity contrasts, the series is observed to converge and the first-order scattered potential is a reasonable approximation to the true secondary potential. We show that the weak-form differential scattering series should theoretically converge given a small perturbation in the conductivity field. The size of this perturbation depends on both the magnitude and spatial distribution of the conductivity contrasts. We provide a convergence criterion based on the matrix norm of the discrete weak-form differential operators.

For small conductivity contrasts, the linearized form of the Fréchet derivative (which is equivalent to the first-order scattered solution) and any associated iterative inverse model update remain valid approximations for implementing sensitivity calculations for non-linear inversion of DC resistivity data. In an iterative non-linear inverse problem, the validity of the linearization depends on the strength of the model perturbation. If the model perturbation is large, the linearized mapping obtained via a Taylor series expansion is not valid. Conversely, model perturbations that are too small make the inversion procedure expensive. For a chosen perturbation, convergence of the differential scattering series can be used to justify linearization about the current model update. Thus, the convergence criterion associated with our formulation of the differential scattering series provides an indirect method of obtaining a measure of how large a model perturbation can be before violating the assumption of linearity. The criterion can therefore be used in deciding the bounds on the step sizes of model updates for the inverse problem.

Although the convergence criterion has potential applicability, we do not necessarily recommend implementation of the full forward differential scattered series (just as the integral scattering solution is rarely used for practical forward modelling) due to the minimal gain/cost ratio achieved through this procedure. In some cases, however, the scattering formulation can provide useful insight into the DC resistivity experiment with regard to charge accumulation across contrasts in electrical conductivity and, in turn, the generation of secondary sources. For large-scale practical problems, the surface charge distribution in 3D can provide intuitive understanding between the observed data and conductivity structures in the subsurface. To elucidate this connection between the scattered potential and charge accumulation, we derive a weak-form equation that relates surface charge density directly to the scattered and total secondary potentials in 3D. The latter relationship is valid for any magnitude or

distribution of secondary conductivity since it is obtained using the non-approximate secondary potential. Computationally, the procedure presented to compute surface charge density is more efficient than an integral equation approach where a dense Green's function needs to be evaluated and integrated along conductivity contrasts.

ACKNOWLEDGEMENTS

This research was funded by the Inland Northwest Research Alliance (SSGP), the Natural Sciences and Engineering Research Council of Canada (PGS B), EPA grant X970085-01-0 and NSF-EPSCOR grant EPS0132626. We thank D.W. Oldenburg, R. Shekhtman and the UBC-GIF for providing DCIP3D, M.D. Knoll for helpful discussions, and the Editor and two anonymous reviewers for their comments and suggestions that resulted in an improved manuscript.

REFERENCES

DCIP3D 2004. *A Program Library for Forward Modelling and Inversion of DC Resistivity and Induced Polarization Data Over 3D Structures, Version 2.0*. Developed under the consortium research project: Inversion of 3D resistivity and induced polarization data. UBC Geophysical Inversion Facility, University of British Columbia.

Dey A. and Morrison H.F. 1979. Resistivity modeling for arbitrarily shaped three-dimensional structures. *Geophysics* **44**, 753–780.

Golub G.H. and Van Loan C.F. 1996. *Matrix Computations*, 3rd edn. John Hopkins University Press, ISBN 0801854148.

Hohmann G.W. and Raiche A.P. 1988. Inversion of controlled-source electromagnetic data. In: *Electromagnetic Methods in Applied Geophysics*, Vol. 1 (ed. M.N. Nabighian), pp. 469–503. Investigations in Geophysics **3**. Society of Exploration Geophysicists, ISBN 1560800690.

Li Y. and Oldenburg D.W. 1991. Aspects of charge accumulation in d.c. resistivity experiments. *Geophysical Prospecting* **39**, 803–826.

Li Y. and Oldenburg D.W. 2000. 3-D inversion of induced polarization data. *Geophysics* **65**, 1931–1945.

Li Y. and Spitzer K. 2002. Three-dimensional DC resistivity forward modelling using finite elements in comparison with finite-difference solutions. *Geophysical Journal International* **151**, 924–934.

Lowry T., Allen M.B. and Shive P.N. 1989. Singularity removal: A refinement of resistivity modeling techniques. *Geophysics* **54**, 766–774.

McGillivray P.R. 1992. *Forward modeling and inversion of DC resistivity and MMR data*. PhD thesis, University of British Columbia.

McGillivray P.R. and Oldenburg D.W. 1990. Methods for calculating Fréchet derivatives and sensitivities for the non-linear inverse problem: A comparative study. *Geophysical Prospecting* **38**, 499–524.

Press W.H, Teukolsky A.A., Vetterling W.T. and Flannery B.P. 1992. *Numerical Recipes in Fortran 77, The Art of Scientific Computing*, 2nd edn. Cambridge University Press, ISBN 052143064X.

Snyder D.D. 1976. A method for modeling the resistivity and IP response of two-dimensional bodies. *Geophysics* **41**, 997–1015.

Spitzer K. 1995. A 3-D finite difference algorithm for DC resistivity modelling using conjugate gradient methods. *Geophysical Journal International* **123**, 903–914.

Spitzer K. 1998. The three-dimensional DC sensitivity for surface and subsurface sources. *Geophysical Journal International* **134**, 736–746.

Spitzer K., Chouteau M. and Boulanger O. 1999. Grid-independent electrode positioning for 3D DC resistivity and IP forward modeling. 2nd International Symposium on Three Dimensional Electromagnetics, Salt Lake City, UT, USA, Extended Abstracts, 189–192.

Spitzer K. and Wurmstich B. 1999. Speed and accuracy in 3-D resistivity modeling. In: *Three-Dimensional Electromagnetics* (eds M. Oristaglio and B. Spies), pp. 161–176. Geophysical Developments **7**. Society of Exploration Geophysicists, ISBN 1560800798.

Telford W.M., Geldart L.P. and Sheriff R.E. 1990. *Applied Geophysics*, 2nd edn. Cambridge University Press, ISBN 0521339383.

Wu X., Xiao Y., Qi C. and Wang T. 2003. Computations of secondary potential for 3D resistivity modelling using an incomplete Choleski conjugate-gradient method. *Geophysical Prospecting* **51**, 567–577.

Zhao S. and Yedlin M.J. 1996. Some refinements on the finite-difference method for 3-D dc resistivity modeling. *Geophysics* **61**, 1301–1307.

Zhou B. and Greenhalgh S.A. 2001. Finite element three-dimensional direct current resistivity modelling: Accuracy and efficiency considerations. *Geophysical Journal International* **145**, 679–688.

APPENDIX

In terms of the discrete linear operators, (11) can be written as

$$\mathbf{C}^{\mathrm{P}}\mathbf{v}^{\mathrm{S}} = -\mathbf{C}^{\mathrm{S}}\mathbf{v} = -\mathbf{C}^{\mathrm{S}}(\mathbf{v}^{\mathrm{P}} + \mathbf{v}^{\mathrm{S}}). \tag{A1}$$

The scattering series then involves updating the scattered potential in an iterative fashion according to

$$\mathbf{C}^{\mathrm{P}}\mathbf{v}^{\mathrm{S}}_{k} = -\mathbf{C}^{\mathrm{S}}\left(\mathbf{v}^{\mathrm{P}} + \mathbf{v}^{\mathrm{S}}_{k-1}\right). \tag{A2}$$

In terms of inverse operators, we can write sequential estimates of the scattered potential as

$$\begin{aligned}
\mathbf{v}^{\mathrm{S}}_{1} &= -(\mathbf{C}^{\mathrm{P}})^{-1}\mathbf{C}^{\mathrm{S}}\left[\mathbf{v}^{\mathrm{P}} + \mathbf{v}^{\mathrm{S}}_{0}\right], \\
\mathbf{v}^{\mathrm{S}}_{2} &= -(\mathbf{C}^{\mathrm{P}})^{-1}\mathbf{C}^{\mathrm{S}}\left[\mathbf{v}^{\mathrm{P}} + \mathbf{v}^{\mathrm{S}}_{1}\right] \\
&= -(\mathbf{C}^{\mathrm{P}})^{-1}\mathbf{C}^{\mathrm{S}}\left[\mathbf{v}^{\mathrm{P}} - (\mathbf{C}^{\mathrm{P}})^{-1}\mathbf{C}^{\mathrm{S}}\left[\mathbf{v}^{\mathrm{P}} + \mathbf{v}^{\mathrm{S}}_{0}\right]\right], \\
\mathbf{v}^{\mathrm{S}}_{3} &= -(\mathbf{C}^{\mathrm{P}})^{-1}\mathbf{C}^{\mathrm{S}}\left[\mathbf{v}^{\mathrm{P}} + \mathbf{v}^{\mathrm{S}}_{2}\right] \\
&= -(\mathbf{C}^{\mathrm{P}})^{-1}\mathbf{C}^{\mathrm{S}}\left[\mathbf{v}^{\mathrm{P}} - (\mathbf{C}^{\mathrm{P}})^{-1}\mathbf{C}^{\mathrm{S}}\left[\mathbf{v}^{\mathrm{P}} - (\mathbf{C}^{\mathrm{P}})^{-1}\mathbf{C}^{\mathrm{S}}[\mathbf{v}^{\mathrm{P}}\right.\right.\right. \\
&\quad \left.\left.\left. + \mathbf{v}^{\mathrm{S}}_{0}]\right]\right], \quad \ldots, \\
\mathbf{v}^{\mathrm{S}}_{k} &= -(\mathbf{C}^{\mathrm{P}})^{-1}\mathbf{C}^{\mathrm{S}}\left[\mathbf{I} - (\mathbf{C}^{\mathrm{P}})^{-1}\mathbf{C}^{\mathrm{S}} + \left((\mathbf{C}^{\mathrm{P}})^{-1}\mathbf{C}^{\mathrm{S}}\right)^{2} - \ldots\right]\mathbf{v}^{\mathrm{P}} \\
&\quad + (-1)^{k}\left((\mathbf{C}^{\mathrm{P}})^{-1}\mathbf{C}^{\mathrm{S}}\right)^{k}\mathbf{v}^{\mathrm{S}}_{0},
\end{aligned} \tag{A3}$$

where $\mathbf{I}$ is the identity matrix.

Since $\mathbf{v}_0^{\mathrm{S}} = 0$, the second term of the kth-order scattered potential becomes zero. Further, for $||(\mathbf{C}^{\mathrm{P}})^{-1}\ \mathbf{C}^{\mathrm{S}}\ || < 1$, and provided that k is large enough, the first term of the kth-order scattered potential can be represented by a binomial expansion, such that we can write

$$\mathbf{v}_k^{\mathrm{S}} = -(\mathbf{C}^{\mathrm{P}})^{-1}\mathbf{C}^{\mathrm{S}}\left[\mathbf{I} + (\mathbf{C}^{\mathrm{P}})^{-1}\mathbf{C}^{\mathrm{S}}\right]^{-1}\mathbf{v}^{\mathrm{P}}. \tag{A4}$$

The requirement that $||(\mathbf{C}^{\mathrm{P}})^{-1}\mathbf{C}^{\mathrm{S}}|| < 1$ for large k is equivalent to the requirement that $||(\mathbf{C}^{\mathrm{P}})^{-1}\mathbf{C}^{\mathrm{S}}||^k \to 0$ as $k \to \infty$, which implies that the matrix $(\mathbf{C}^{\mathrm{P}})^{-1}\mathbf{C}^{\mathrm{S}}$ is itself convergent with a spectral radius of less than unity. To demonstrate that the series (A3) indeed converges for large k, we show that (A4) is exact in the following manner (dropping the subscript k):

$$\begin{aligned}
\mathbf{C}^{\mathrm{P}}\mathbf{v}^{\mathrm{S}} &= -\mathbf{C}^{\mathrm{S}}[\mathbf{I} + (\mathbf{C}^{\mathrm{P}})^{-1}\mathbf{C}^{\mathrm{S}}]^{-1}\mathbf{v}^{\mathrm{P}},\\
\mathbf{v}^{\mathrm{S}} &= -(\mathbf{C}^{\mathrm{P}})^{-1}\mathbf{C}^{\mathrm{S}}[\mathbf{I} + (\mathbf{C}^{\mathrm{P}})^{-1}\mathbf{C}^{\mathrm{S}}]^{-1}\mathbf{v}^{\mathrm{P}},\\
\mathbf{C}^{\mathrm{S}}\mathbf{v}^{\mathrm{S}} &= -\mathbf{C}^{\mathrm{S}}(\mathbf{C}^{\mathrm{P}})^{-1}\mathbf{C}^{\mathrm{S}}[\mathbf{I} + (\mathbf{C}^{\mathrm{P}})^{-1}\mathbf{C}^{\mathrm{S}}]^{-1}\mathbf{v}^{\mathrm{P}},\\
\mathbf{C}\mathbf{v}^{\mathrm{S}} &= \mathbf{C}^{\mathrm{P}}\mathbf{v}^{\mathrm{S}} + \mathbf{C}^{\mathrm{S}}\mathbf{v}^{\mathrm{S}},\\
\mathbf{C}\mathbf{v}^{\mathrm{S}} &= \\
&\quad -\mathbf{C}^{\mathrm{S}}\{(\mathbf{C}^{\mathrm{P}})^{-1}\mathbf{C}^{\mathrm{S}}[\mathbf{I} + (\mathbf{C}^{\mathrm{P}})^{-1}\mathbf{C}^{\mathrm{S}}]^{-1} + [\mathbf{I} + (\mathbf{C}^{\mathrm{P}})^{-1}\mathbf{C}^{\mathrm{S}}]^{-1}\}\mathbf{v}^{\mathrm{P}},\\
\mathbf{C}\mathbf{v}^{\mathrm{S}} &= -\mathbf{C}^{\mathrm{S}}[(\mathbf{C}^{\mathrm{P}})^{-1}\mathbf{C}^{\mathrm{S}} + \mathbf{I}][\mathbf{I} + (\mathbf{C}^{\mathrm{P}})^{-1}\mathbf{C}^{\mathrm{S}}]^{-1}\mathbf{v}^{\mathrm{P}},\\
\mathbf{C}\mathbf{v}^{\mathrm{S}} &= -\mathbf{C}^{\mathrm{S}}\mathbf{v}^{\mathrm{P}}.
\end{aligned} \tag{A5}$$

The final form of (*A5*) is equivalent to the stable, non-approximate secondary formulation of (9). It follows that the scattered series converges: in the limit $\mathbf{v}_k^{\mathrm{S}} \to \mathbf{v}^{\mathrm{S}}$ as $k \to \infty$, provided that $||(\mathbf{C}^{\mathrm{P}})^{-1}\mathbf{C}^{\mathrm{S}}\ || < 1$ or the spectral radius of $(\mathbf{C}^{\mathrm{P}})^{-1}\mathbf{C}^{\mathrm{S}}$ is less than unity.